Long-Wavelength Quantum Well Infrared Photodetectors

M. Razeghi, M. Erdtmann, C. Jelen, J. Diaz and F. Guastavino

Northwestern University, Evanston, IL 60 208

and

Y.S. Park

Office of the Naval Research, 800 N. Quincy St., Arlington, VA 22 217-5 660

ABSTRACT

A majority of IR sensors used for imaging arrays operating in the long-wavelength IR region between 8 μm–12 μm are based on mercury cadmium telluride (*HgCdTe*). This material system is unable to satisfy all the requirements imposed by modern applications. Structural difficulties due to poor uniformity, high defect densities, and weak bond strengths cause difficulties in manufacturing large IR focal plane array cameras. As an alternative, quantum well infrared photodetectors (QWIPs) utilising intersubband absorption between gallium arsenide (*GaAs*) wells and aluminium gallium arsenide (*AlGaAs*) barriers were perfected. These QWIPs possess better uniformity in comparison to *HgCdTe* detectors, and QWIP imaging arrays have recently become commercially available. However, the responsivity of *GaAs/AlGaAs* QWIPs is still lower than *HgCdTe* detectors. To further improve the responsivity of QWIP detectors, QWIPs with wells or barriers of *GaInAsP* instead of *AlGaAs* have been developed. Results of QWIPs made from the material systems *GaAs/GaInP*, *GaInAs(P)/InP*, *(Al)GaInAs/InP*, and *GaInAs/AlInAs* have been discussed.

Keywords: Infrared detectors, quantum well infrared detectors, QWIP detectors, QWIP imaging arrays, multi-quantum well structures, two-colour detectors, LWIR detectors

1. INTRODUCTION

The ability to detect and process IR radiation can provide wealth of information about an object that is not available in other regions of the spectrum. One type of recently developed detector that can cover most of the IR spectrum is the quantum well infrared photodetector (QWIP). Using intersubband absorption within a quantum well (QW), a QWIP can be designed with relatively wide band gap materials yet be sensitive to low energy photons in the IR region.

Interestingly, despite the long history of IR detectors, QWIPs have been recently developed. The idea of using QWs for IR detection was first presented by Esaki and Sakaki[1], in 1977. Eight years later, West and Eglash[2] made the first experimental observation of strong intersubband absorption in a *GaAs/AlGaAs* multi-QW (MQW) structure. In 1987, the first QWIP device based on intersubband absorption, also made from a *GaAs/AlGaAs* MQW structure, was demonstrated by Levine[3], *et al.* Since that time, QWIP technology

Table 1. Properties of material systems for QWIP fabrication in the wavelength range 8 μm–9 μm

Material system	GaAs/AlGaAs	GaAs/GaInP	GaInAs/InP
Barrier material	AlGaAs (ternary)	GaInP (ternary)	InP (binary)
Well mobility at 300K ($cm^2V^{-1}s^{-1}$)	9000	9000	13 500
Barrier mobility at 300K ($cm^2V^{-1}s^{-1}$)	2000	3500	5500
Well electron effective mass (m^*/m_0)	0.067	0.067	0.041

has developed rapidly to the point that it has reached commercial maturation[4].

QWIPs also have been fabricated from numerous groups III-V material systems other than GaAs/AlGaAs, including GaAs/GaInP, GaInAs(P)/InP, and (Al)GaInAs/InP. Table 1 shows three material systems and some of their properties from which QWIPs in the wavelength (λ) = 8 μm–9 μm range have been demonstrated. Better results have been achieved with the GaInAs/InP material system, since it offers a higher well and barrier mobility, a lower well electron effective mass, and a binary barrier with an inherently lower defect density[5-8].

Another disadvantage of GaAs/AlGaAs QWIPs is that perpendicular carrier transport rapidly degrades when the $Al_xGa_{1-x}As$ barrier becomes indirect gap (for $x > 0.45$). For this reason, the short wavelength infrared (SWIR) detector possible with this material system[9] is ~ 6 μm. Thus, the need to achieve mid-wavelength (MW) absorption has lead to studies of other material systems[10-11], such as $In_{0.2}Ga_{0.8}As/Al_{0.38}Ga_{0.62}As$, and $In_{0.53}Ga_{0.47}As/Al_{0.48}In_{0.52}As$. These material systems avoid the use of indirect gap AlGaAs barriers.

For some applications, especially for tunnelling devices, $In_{0.53}Ga_{0.47}As/Al_{0.48}In_{0.52}As$ MQWs lattice-matched to InP substrates have several advantages in comparison to structures composed of $InGaAs/Al_xGa_{1-x}As$, where x is small enough to ensure a direct energy gap in the AlGaAs barrier material. The effective mass of the electrons, which governs the drift mobility and tunnelling

properties, amounts to 0.041 m_0 in InGaAs as compared to 0.053 m_0 in $In_{0.2}Ga_{0.8}As/AlGaAs$, where m_0 is the free electron mass. The mid-wavelength infrared (MWIR) InGaAs/AlInAs QW detector is lattice-matched with long-wavelength infrared (LWIR) InGaAs/InP QWIP detectors, allowing a two-colour lattice-matched detector stack to be grown on InP.

The demand for automatic target detection, definition, and recognition is mandatory for the development of dual wavelength forward looking infrared (FLIR) sensor arrays. Two-colour IR detectors designed for dual-band applications require MWIR and LWIR focal plane arrays (FPAs) to be monolithically integrated on a single substrate. This objective has been difficult to achieve due to the lattice mismatch between commonly used interband MWIR and LWIR IR materials, such as InSb and HgCdTe. For this reason, stacks of lattice-matched MQW intersubband photodetectors have been proposed for use in multi-colour IR detectors.

2. QUANTUM WELL INFRARED PHOTODETECTORS

The most popular material for IR detection is the groups II-VI alloys, chiefly HgCdTe. Because of the extensive research carried out on HgCdTe, it is the standard against which all other IR photon detectors are matched. Where the material shines is its quantum efficiency and detectivity[12]: At 77K, quantum efficiency has been reported exceeding 70 per cent and detectivity exceeding 10^{12} $cmHz^{1/2}W^{-1}$. FPAs as large as 640 × 480 have been made that can detect either in the MWIR or LWIR region and are compatible with silicon ROIC[13].

Despite these results, a serious problem exists with the alloy that makes the production of HgCdTe detectors troublesome. While the fundamental properties of the material are favourable, the technology of producing HgCdTe material and detectors is far from reliable. HgCdTe, as an alloy, is not stable: There is a segregation of the constituent binaries during crystallisation and the bonding between mercury and telluride is weak, facilitating defect formation and mercury migration. The uniformity and reproducibility of a HgCdTe film

is poor[14], and passivation is required to process detectors. The end result of using this material is low yield and high cost detector arrays.

To take advantage of the superior material growth and technology that exists with the wide band gap materials, such as *AlGaAs/GaAs* or *GaInAs/InP*, a different mechanism is employed for detection in the MWIR or LWIR region. While interband absorption in these materials occurs only in the SWIR or visible regions of the spectrum, intersubband absorption, through the use of QWs, can make longer wavelength detection possible. The process is shown in Fig. 1.
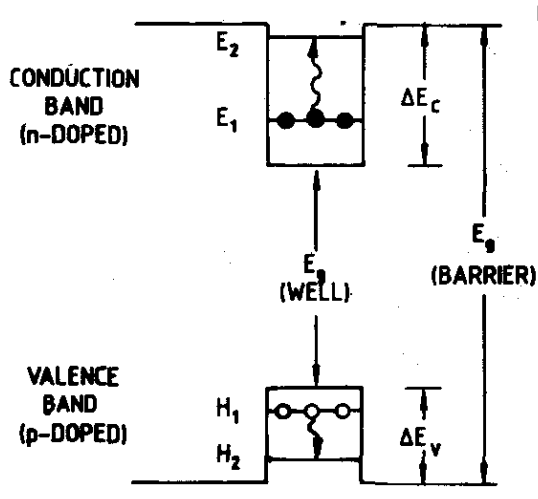

Figure 1. Intersubband absorption which takes place entirely within the valence band (H_1 to H_2) or conduction band (E_1 to E_2) of a QW.

QW consists of a very thin layer, < 100 Å, of a smaller band gap material (the well), sandwiched with a larger band gap material (the barrier). This produces a particle-in-the-box phenomenon where the allowed energy states inside the well are confined to bound levels. Absorption takes place from one bound level in the QW to another, as seen in Fig. 2. The energy separation between the two bound levels, E_1 and E_2 or H_1 and H_2, is much smaller than the band gap of either the well or barrier material, hence the intersubband absorption wavelength is much longer.

One requirement for detection using QWs is that the well material must be doped. Because the energy of an absorbed photon is less than the band gap, it cannot produce an excited photocarrier by
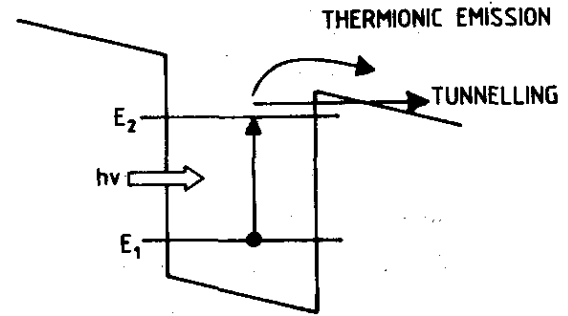

Figure 2. A bound-to-bound state transition, showing two possible ways a photocarrier can escape the well: Tunnelling and thermionic emission.

itself. With the addition of carriers in the well, excitation only needs to happen from the first bound state to the next bound state. For n-type doping, excitation occurs entirely within the conduction band; for p-type doping, excitation occurs entirely within the valence band.

The integrated absorption strength of a MQW structure is given by

$$\int_0^\infty \alpha(\nu)d\nu = \left(\frac{\rho_c N_w q^2 h f}{4\varepsilon_0 m^* c n_r}\right)\left(\frac{\sin^2\theta}{\cos\theta}\right) \qquad (1)$$

where $\alpha(\nu)$ is the absorption spectrum, ν is the frequency, $\rho_c = N_d L_w$ is the two-dimensional carrier density in the well, N_d is the three-dimensional carrier density, L_w is the well width, N_w is the number of doped wells in the structure, q is the charge of an electron, h is Planck's constant, f is the oscillator strength, ε_0 is the permittivity of free space, m^* is the electron effective mass in the well, c is the speed of light, n_r is the refractive index of the well material, and θ is the angle between the incident light and direction perpendicular to the QWs.

f is proportional to the square of the optical matrix element $<z>$, where z represents the direction perpendicular to the QWs. This, along with the fact that the absorption strength is proportional to $\sin^2\theta/\cos\theta$ implies a serious constraint of QW absorption: The electric field of the incident light must have a component parallel to z for absorption to occur. Therefore, the direction of the incident light cannot be normal to the QWs—when $\theta = 0°$— and must come in at an angle.

It is noted that this quantum mechanical selection rule for absorption only applies to QWs that are doped *n*-type. For *p*-type QWs, there is strong mixing amongst the heavy holes and light holes in the valence band which can make absorption of normal incidence light possible[15].

Photocurrent is produced when an excited photocarrier is able to escape the well whereupon an externally applied bias can sweep it out to be collected by one of the contacts. Based on the properties of the QW, like the well thickness and depth, the absorption spectrum can be tailored for detection at a particular range of wavelengths. Based on this information, the reasoning for the name quantum well infrared photodetector (QWIP) becomes evident.
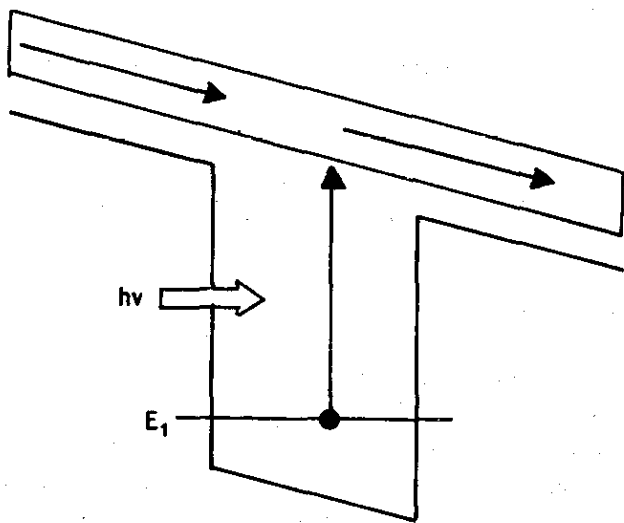

Figure 3. A bound-to-continuum state transition

The first type of QWIPs produced had intersubband absorption occurring between two bound states contained within the QW, similar to the levels E_1 and E_2 shown in Fig. 1. In this case, when the QW contains two or more bound states, the QWIP is known as a bound-to-bound state QWIP. When a carrier absorbs a photon and jumps up to the second bound state, it still needs a way to escape from the well and get swept out. The two possible ways are shown in Fig. 2. The first is by tunnelling through the barrier, and the second is by thermionic emission, where the carrier is thermally excited out of the well. For a bound-to-bound state QWIP, tunnelling usually dominates, and this only

happens when the applied electric field is sufficiently large.

A serious problem experienced with bound-to-bound state QWIP is the excessive amount of dark current (I) generated in the detector. The same mechanisms that produce photocurrent in a bound-to-bound state QWIP, tunnelling and thermionic emission, can also produce dark current. The difference is that dark current is created in the absence of photon absorption. It relates to the structure of a bound-to-bound state QWIP. Since the bulk of the photocarriers tunnel out of the QW, it is advantageous to have thinner barriers to facilitate tunnelling. Additionally, a large electric field is needed for tunnelling to occur at a tolerable rate. The combination of these two factors allows random carriers in the well to also tunnel out, producing a relatively large dark current.

The way to circumvent this is to have the excited photocarriers escape the QW without tunnelling. By making the QWs thinner, the energy level of the second bound state is raised enough so that it is completely out of the well and into the continuum band. When a carrier becomes excited, it jumps from the first bound state in the well to the contiuum state above the well. Once there, it is readily swept out.

The bound-to-continuum transition is shown in Fig. 3. The barriers can be much thicker in this type of structure, which dramatically reduces[16] dark current. Also, the large electric field required in the bound-to-bound state QWIP is no longer needed, further reducing dark current. In this case, when the QW contains only one bound state, the QWIP is known as a bound-to-continuum state QWIP. Another feature of a bound-to-continuum state QWIP is that it has a much broader absorption spectrum than a bound-to-bound state QWIP since the continuum level exists over a larger spread of energy.

3. QWIP PERFORMANCE

3.1 *GaAs/GaInP* QWIPs

GaAs/GaInP *n*-type QWIP ($\lambda = 8$ µm–20 µm) structures were grown using gas source molecular beam epitaxy (GSMBE) on (100) semi-insulating *GaAs* substrates. *GaAs* well widths were 40Å, 65Å,

and 75Å, for samples A, B and C, respectively and the lattice-matched $Ga_{0.51}In_{0.49}P$ barriers were 500 Å. Each sample superlattice (SL) had 20 periods. The silicon doping in the QWs was 5×10^{17} cm^{-3}.

The photoresponse for three well widths is shown in Fig. 4. The peak wavelengths of the three samples were: 10.4 µm, 12.78 µm, and 13.3 µm for well widths of 40 Å, 65 Å and 75 Å respectively. The cut-off wavelengths were: 13.5 µm, 15 µm, and 15.5 µm, respectively for the three samples. The full width at half maximum (FWHM) for the three samples in meV (and as $\Delta\lambda/\lambda$) were 185 meV (0.58), 37 meV (0.5) and 42 meV (0.375), respectively. These FWHM are typical for bound-to-continuum state QWIPs. The reduction in FWHM for wider wells indicates that the second excited state in these samples is closer to resonance with the barrier energy. At low bias, where tunnelling can be neglected, dark current is expected to increase exponentially with temperature following Eqn (2) as

$$I \propto T \exp\left(-\frac{\Delta E}{kT}\right) \tag{2}$$

Therefore, the activation energy (ΔE) can be obtained by calculating the slope of log (I/T) versus $1/kT$. For the three samples with 40Å, 65Å and 75Å wells, the ΔEs are 37 meV, 50 meV and 46 meV, respectively.
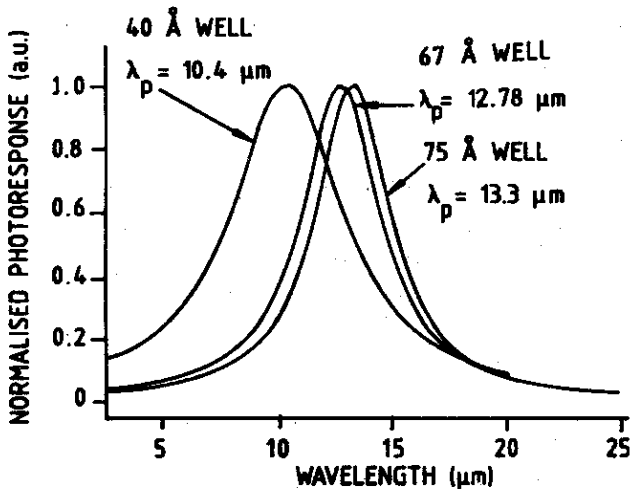
QW sub-band energies were determined using

Table 2. Calculation of conduction band offset. $\Delta E_C = (E_0 - E_{EXCH}) + E_F + \Delta E$

Well (Å)	$E_0 - E_{EXCH}$	(ΔE)	(E_F)	(ΔE_c)
40	79	37	4.4	120.4
65	62	50	10.4	122.4
75	59	46	12.5	120.5

a four-band Kane model, which includes the effects of band non-parabolicity and band mixing. The electron-electron exchange interaction effect was also included, and the depolarisation and exciton shifts were neglected as before.

From these sub-band energy levels and dark current activation energies, we computed the conduction band offset ΔE_c [$\Delta E_c = (E_0 - E_{EXCH}) + E_F + \Delta E$, where E_0 is the ground state energy, E_{EXCH} is the electron-electron interaction energy, E_F is the Fermi energy, and ΔE is the activation energy] to be 121.1 meV $\pm$ 2 meV. Data used in this model is given in Table 2. From the known band gaps of *GaAs* and *GaInP*, the band gap difference ΔE_g = 483 meV has been obtained. Using the experimentally determined conduction band offset, a band offset ratio, $\Delta E_c/\Delta E_g$ = 0.251 has been calculated, which matches the assumed ratio used for theoretical modelling. Values of ΔE_c in the literature range between 80 meV to 240meV. However, the only previous measurement for material grown[18] by GSMBE was 108 meV. This experimental result agrees well with previous results.
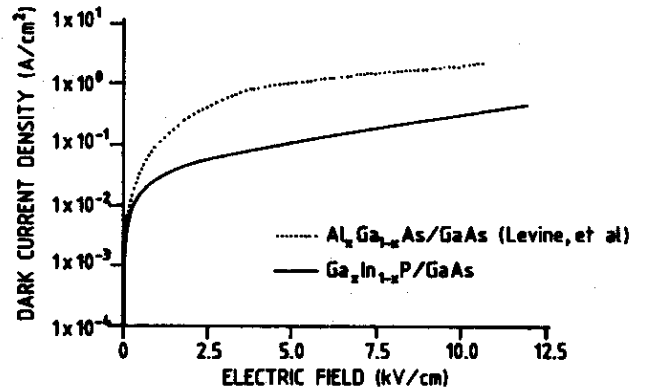
The dark current density (A/cm^2) at 77K for

Figure 4. Normalised optical response at 77K for samples with 40 Å, 65 Å and 75 Å QWs.

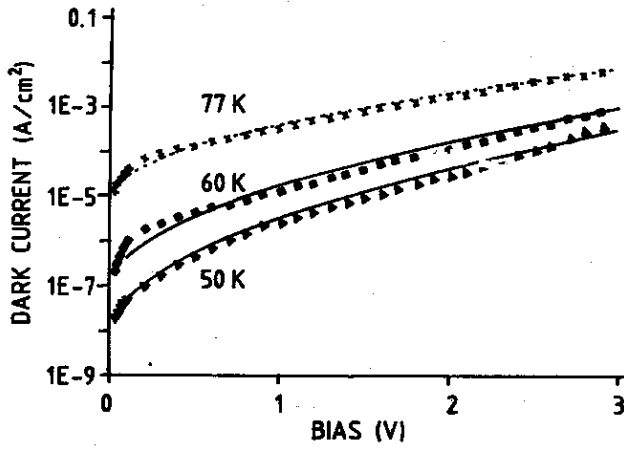**Figure 5.** Measured dark current density for sample B compared to *GaAs/AlGaAs* results[7].

39

Figure 6. Comparison of experimental (points) and theoretical (lines) dark current-voltage curves at various temperatures for sample B.

Figure 7. Calculated gain and recombination lifetimes as a function of applied bias for sample B.

sample B as a function of electric field (V/cm) is shown in Fig. 5. The results of Levine[9] for a *GaAs/ AlGaAs* QWIP with similar well doping density, and cut-off wavelength is shown for comparison. The smaller dark current may be due to *GaAs/ $Ga_xIn_{1-x}P$*'s larger mobility[19], smaller surface recombination velocity[20], or smaller interface roughness[21], by comparison to *$GaAs/Al_xGa_{1-x}As$*.

We have modelled the dark current assuming thermodynamic carrier equilibrium and a drift model[22] where the drift velocity is proportional to the electric field according to

$$v_d = \frac{\mu V}{L_b}\left[1 + \left(\frac{\mu V}{v_s L_p}\right)^2\right]^{-1/2}$$

(3)

where μ is the mobility, V is the applied bias per QW, L_b is the barrier width and L_p is the period thickness. We have neglected any complication to do with the way in which carriers in the QW are replenished and the mechanisms of charge transfer from the emitter contact to the MQW. Since the carriers which are thermally excited into the continuum transport states and contribute to the dark current are originally from the QWs, a 2-D density of states is used.

For calculating the transmission coefficient $T(E,V)$, we have used $T(E,V) = 1$ for E larger than
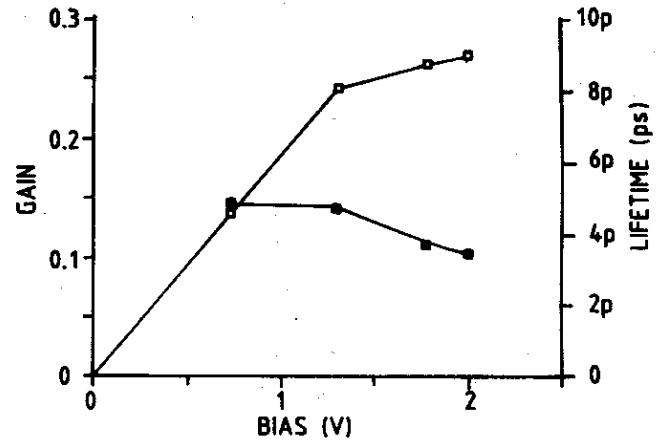
the conduction band offset V_o and the Wentzel-Kramers-Brillouin (WKB) approximation[23] for $E < V_o$. In the calculation, we took the conduction band offset V_o to be 0.1 eV[24]. Conduction band non-parabolicity was neglected because it had a negligible effect[22] on dark current, but image charge effects have been included.

The dark current measurements for the 65 Å well sample are shown as a function of voltage and temperature and compared with the calculated values in Fig. 6. Good agreement is achieved as a function of both bias and temperature over seven orders of magnitude in dark current. These calculations use a drift mobility of 1000 cm²V⁻¹s⁻¹, a saturation velocity of 1.5 x 10⁵ cm⁻¹ and the nominal sample parameters shown in Table 2. The saturation velocity is approximately one order of magnitude lower than typical values for bulk *GaInP* at 77K[25,26] in a similar electric field, as would be expected because of re-trapping by QWs and interface scattering.

The photoconductive gain is a ratio of the distance (*l*) travelled by an electron before recapture to the thickness of the device L. At the biases used in this experiment, $l = v_d(E)\tau$ and therefore

$$g = v_d(E)\tau/L$$

(4)

To evaluate the carrier lifetimes in these *GaAs/ GaInP* detectors, we directly measured the noise current as a function of bias using a spectrum analyser at $T = 77K$. This noise is dominated by

generation-recombination noise at $T = 77K$. From the equation for G-R noise, $i_{G-R} = \sqrt{4qI_d g \Delta f}$, we first calculated the gain using dark current-bias data from Fig. 6, and then calculated the carrier lifetimes using Eqn (4). Figure 7 shows the carrier lifetimes and gain derived from noise measurements for the 65 Å well sample.

3.2. GaInAs/InP QWIPs

The specific detectivity (D^*) of GaInAs/InP QWIPs can be expressed in terms of the Fermi level[27] as

$$D^* \propto E_F \exp\left(-\frac{E_F}{2kT}\right) \tag{5}$$

where k is Boltzmann's constant, T is temperature, and E_F is the QW Fermi level. D^* has a maximum value when $E_F = 2kT$. When $T = 80K$, the optimal value of E_F is 13.8 meV.

While GaInAs/InP QWIPs have been grown by metallo-organic molecular beam epitaxy (MOMBE)[7], liquid phase-metallo-organic chemical vapour deposition[8] (LP-MOCVD), and GSMBE[28], little work has been done to optimise the performance of GaInAs/InP QWIPs. In this section, the influence of the GaInAs QW doping density on responsivity, dark current, noise current, and detectivity has been reported for GaInAs/InP QWIPs ($\lambda = 9$ μm) grown by LP-MOCVD.

All epitaxy for this study took place inside an LP-MOCVD reactor[29]. Triethylgallium and trimethylindium are the group III sources, arsine and phosphine are the group V sources, and silane is the n-type dopant. The growth temperature was 480 °C and the growth pressure was 78 torr. We grew three series of GaInAs/InP QWIPs with three different QW doping densities whose structures contained 20 QWs of 60 Å n-GaInAs surrounded by 500 Å undoped InP barriers on semi-insulating InP substrate; these structures have been designed for detection in the $\lambda = 8$ μm–9 μm range. On each side of the well region are a 0.50 μm top and a 0.75 μm bottom n-GaInAs contact layers doped to 1×10^{18} cm^{-3}. The outermost 5 Å of each QW were undoped to prevent impurity diffusion into
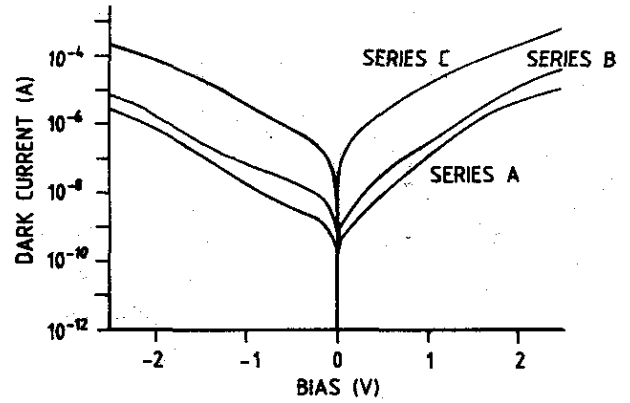

Figure 8. Dark current as a function of bias of the three GaInAs/InP QWIP series.

the barrier. QW doping densities used were 1.7×10^{17} cm^{-3} (series A), 5×10^{17} cm^{-3} (series B) and 1.7×10^{18} cm^{-3} (series C).

After epitaxy, 400 μm × 400 μm mesas were patterned with an electron cyclotron resonance-enhanced reactive ion etch reactor using $BCl_3/Cl_2/Ar$ etch chemistry that yielded approximately 45° sidewalls and then Ti/Pt/Au metal contacts were deposited with electron beam evaporation. The device measurements took place at 80K inside a liquid nitrogen cryostat with normal incidence illumination. The angled mesa sidewalls served to couple the incident light parallel to the QWs and allowed for normal incident illumination.

The dark current, for the three GaInAs/InP QWIP series at $T = 80K$ has been reproduced in Fig. 8. The noise currents were 8.0×10^{-14} AHz$^{-1/2}$, 1.0×10^{-13} AHz$^{-1/2}$, and 1.3×10^{-11} AHz$^{-1/2}$ at a bias of 1 V for series A, B and C, respectively. This trend in both dark current and noise current is due to a substantial increase in the Fermi level with doping, which in turn causes a decrease in ΔE. For series A, B and C, the calculated Fermi levels are 1.7 meV, 16.3 meV and 56.6 meV, respectively, above the first bound state. A detailed description of Fermi level is given elsewhere[30]. The relative spectral responses for the three series is shown in the inset of Fig. 9. Given that each of the three series has the same peak spectral response at $\lambda = 9.0$ μm, and hence the same first bound level energy, then the large increase in the Fermi level is responsible for the drop in activation energy.
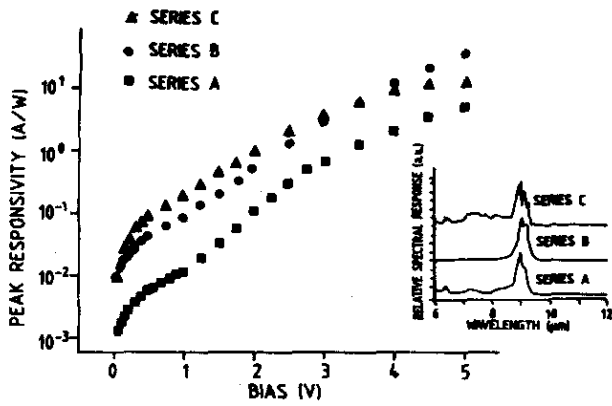
41

Figure 9. Peak responsivity as a function of bias of the three *GaInAs/InP* QWIP series. The inset shows the relative spectral response of the three QWIP series.

To analyse the trend in dark current, one can model the dark current as $I_D = n^* qvA$, where v is the average drift velocity, A is the device area, and the effective number of electrons thermally excited out of the well[31] n^* is:

$$n^* = \frac{m^* kT}{\pi \hbar^2 L_p} \exp\left(-\frac{\Delta E_c - E_1 - E_f}{kT}\right) \qquad (6)$$

where L_p is the period thickness, ΔE_c is the conduction band offset, and E_1 is the energy of the first bound level. It is therefore expected that the ratio of dark current is equal to the ratio of thermally excited carriers from Eqn (6). Between series B and A, the calculated dark current ratio is 3.2, while between series C and B, it is 44. This is in good agreement with the actual dark current ratios: Between series B and A, dark current ratio is 3.5, while between series C and B, it is 61. Over a larger than two order of magnitude change in dark current, the fit is within 30 per cent.

Also, we fabricated two additional QWIPs identical to series A but with 750 Å and 1000 Å *InP* barriers and discovered no significant change in dark current, amongst these three QWIPs as a function of applied electric field. So, it is not advantageous to use thicker barriers to reduce dark current.

The graph of responsivity for the three *GaInAs/InP* QWIP series is shown in Fig. 9. For the case of series B at a bias of 5 V, the responsivity
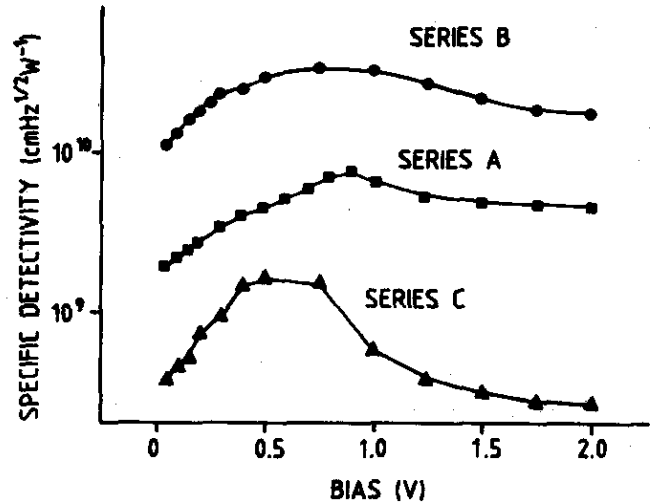

Figure 10. Specific detectivity as a function of bias of the three *GaInAs/InP* QWIP series.

is 33.2 AW^{-1}, which is known to be the largest absolute responsivity and the largest ratio of responsivity to electric field for QWIPs in this wavelength range ($\lambda = 8$ μm–9 μm). From the Fermi levels given above, one can determine the concentration of ionised carriers within each series that are able to contribute to photo-current, and hence the responsivity[32]. Between series B and A, the ratio of ionised carriers is 7.0, which closely matches the measured responsivity ratio of 7.6. The sharp drop in series A most likely is due to the depletion of carriers inside the well because the doping density is critically low. Between series C and B, the ratio of ionised carriers is 3.7, which is somewhat higher than the measured responsivity ratio of 2.2 between the two series.

The detectivity of the three *GaInAs/InP* QWIP series is calculated and plotted in Fig. 10. Since the detectivity is proportional to the responsivity divided by the current noise, series A's detectivity is lower because its responsivity was much lower than the other two series while series C's detectivity is lower because its current noise was much higher than the other two series. Series B has the optimal QW doping density to avoid these two pitfalls, and yields a maximum detectivity of 3.5×10^{10} cmHz$^{1/2}$/W at a bias of 0.75 V. In addition, the Fermi level of 16.3 meV for series B is in excellent agreement with Eqn (5) which states that the optimal Fermi level is 13.8 meV.

The detectivity amongst the three series is very sensitive to doping. By changing the QW doping density by over a factor of 10, the detectivity changes by factor of 20. Thus, it is extremely crucial to fabricate *GaInAs/InP* QWIP with the optimal QW doping density. This is in stark contrast to *GaAs/AlGaAs* QWIP, where changing the QW doping density by over a factor of 30 changed the detectivity by only a factor of two[32].

The much larger sensitivity of detectivity to doping in *GaInAs/InP* QWIP versus that of *GaAs/AlGaAs* QWIP can be explained by Eqn (5). The relationship between the Fermi level and ionised carrier density (N_d) can be approximated by:

$$N_d \approx m^* E_F / \pi \hbar^2 L_w$$

where L_w is the QW thickness. Solving for E_F yields:

$$E_F \approx N_d \pi \hbar^2 L_w / m^*$$

The Fermi level scales with the ionised carrier density as L_w/m^*. The larger the factor L_w/m^* is, the sharper the peak of detectivity as a function of ionised carrier density according to Eqn (5). In other words, the larger the factor L_w/m^* is, the larger the sensitivity of detectivity to ionised carrier density. For *GaInAs/InP* QWIPs, both the well width is larger (60 Å v. 40 Å) and the well effective mass is smaller ($0.041m_0$ v. $0.067m_0$) than for the *GaAs/AlGaAs* QWIPs as described by Gunapala, *et al.* (in Ref. 32). Thus the factor L_w/m^* will be significantly larger, and the sensitivity of detectivity to the doping density will also be larger. This partly

explains the observed difference of the sensitivity of detectivity between the two material systems.

Another difference may be the dependence of carrier lifetime on doping density. Gain values calculated from noise measurements for these samples are 0.4, 1.0, and 10.0 for series A, B and C, respectively, at 1 V bias. Assuming the transit time is approximately the same for QWIPs fabricated from either *GaInAs/InP* or *GaAs/AlGaAs* at equal electric fields, the measured gain values are proportional to the carrier lifetime[33]. The values of gain measured here for *GaInAs/InP* QWIPs vary strongly (by over one order of magnitude) with QW doping density than values measured[32] for the *GaAs/AlGaAs* QWIPs (by a factor of two) for the same range of doping density, and therefore also contribute to the sensitivity of detectivity with doping.

3.3 *AlGaInAs/InP* & *GaInAs/AlInAs* QWIPs

In this section, we demonstrate that high quality QWIPs in both the 3 μm-5 μm and 8 μm-20 μm spectral bands can be grown on *InP* substrate using GSMBE.

The device parameters of the QWIP studied are listed in Table 3, where L_b represents the barrier width, L_w is the well width, and N_d denotes the donor doping concentration of the QWs. The wafers were grown using an EPI modular Gen-II GSMBE system equipped with arsine and phosphine sources for arsenic and phosphorous. Metallic gallium and indium were used for group III elements. The devices were grown on semi-insulating *InP* (100) substrates. After epitaxial

Table 3. Device parameters for measured QWIPs

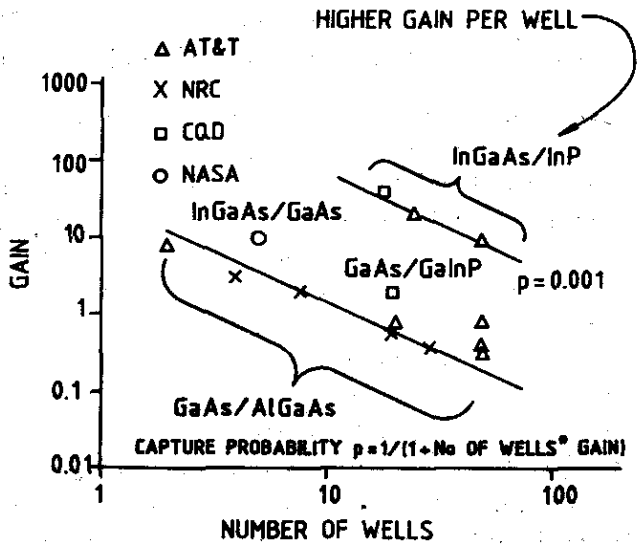| QWIP	Sample A	Sample B	Sample C	Sample D
Barrier material	*InP*	*InP*	*InP*	$Al_{0.48}In_{0.52}As$
L_b (Å)	500	500	500	500
Well material	$In_{0.53}Ga_{0.47}As$	$In_{0.52}Ga_{0.38}Al_{0.1}As$	$In_{0.52}Ga_{0.33}Al_{0.15}As$	$In_{0.53}Ga_{0.47}As$
L_w (Å)	56	60	65	35
N_d (cm^{-3})	5×10^{17}	5×10^{17}	5×10^{17}	2×10^{18}
Periods	20	25	25	25

Figure 11. Photoconductive gain versus number of QWs for various QWIP systems.

growth, standard photolithographic process was used to fabricate mesa photodetectors. A square active area of 1.6 x 10^{-3} cm^2 was defined and 1600Å $AuGe/Ni/Au$ ohmic contacts were deposited by electron beam evaporation and patterned using a lift-off process.

3.3.1 GaInAs/InP QWIPs

The peak responsivity value of 7.5 A/W at 5 V reverse bias for sample A is approximately one order of magnitude higher than that typically obtained in $AlGaAs/GaAs$ QWIP. The maximum D^* of the QWIP measured was found to be 5 x 10^{10} cm √HzW^{-1} at 1.2 V. A comparison of the photoconductive gain measured for different QWIP materials is shown in Fig. 11. The higher gain in InP-barrier QWIP is probably due to the longer carrier lifetime (because of a lower recombination rate) and higher drift velocity in the InP barriers, and perhaps a decrease in the number of scattering centres due to the high quality of the binary barrier material.

The increased gain results in a higher detector responsivity. The responsivity for sample A is larger compared with $GaAs/AlGaAs$ devices[34]. This is shown in Fig. 12.

3.3.2 GaInAs/AlInAs QWIPs

To determine the wavelength range at which $InGaAs/InAlAs$ QWIPs can operate, we have calculated
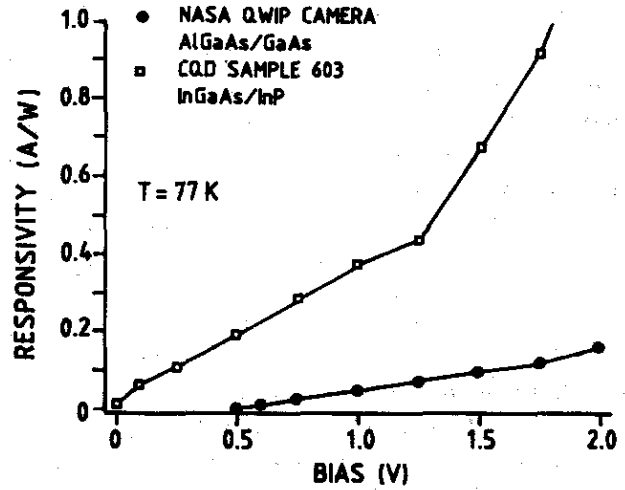

Figure 12. $InGaAs/InP$ QWIP (sample A) responsivity compared to $GaAs/AlGaAs$ QWIP[34].

the energy levels in $InGaAs/AlInAs$ MQW structures. For this calculation, we have assumed $m_{well} = 0.041m_o$, $m_{barrier} = 0.075\ m_o$, $E_{g77K\ well} = 1.508$ eV, $E_{g77K\ barrier} = 0.801$, and $\Delta E_c = 0.5$ meV. In Fig. 13, $n = 1$ and $n = 2$ electron energy levels versus the well width are plotted. The $n = 2$ level is confined to the well for well widths thicker than 35 Å, and is an extended band for narrower wells. For wells thicker than 35 Å, the intersubband absorption energy is plotted as a dashed line calculated from the energy difference between $n = 1$ and $n = 2$ states. For narrower wells, the absorption energy is plotted as a dotted line calculated from the difference
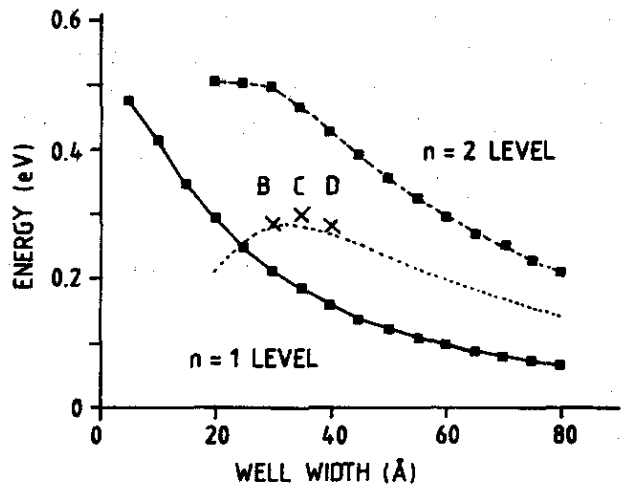

Figure 13. Calculated two first electron levels in $InGaAs/AlInAs$ QWs (solid lines) vs well width. Experimental data points obtained for samples with well widths of 30 Å, 35 Å and 40 Å are shown as well.
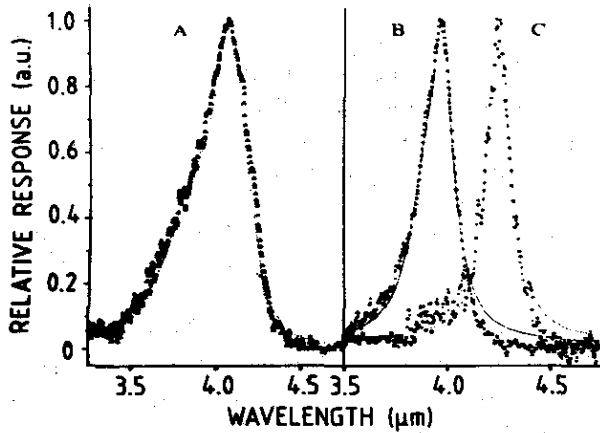
Figure 14. Measured spectral responsivity of the 30 Å, 35 Å and 40 Å QW samples at $T = 77K$ with 1 V reverse bias.

Figure 15. Normalised spectral response for $In_{0.52}(Ga_{1-x}Al_x)_{0.48}As/InP$ QWIPs with $x = 0$, $x = 0.1$, and $x = 0.15$ mole fraction of $AlAs$.

in energy between the confined $n = 1$ and the centre of the continuum band. The experimental data points for samples with QW widths of 30 Å, 35 Å and 40 Å are also shown, demonstrating good agreement with model calculations.

The relative spectral response for the three samples was measured using a Mattson Fourier transform infrared (FTIR) spectrometer. The measurements were made at $T = 77K$ under varying forward and reverse biases. No change in the shape of the spectral response occurred for ± 5 V bias for these samples.

The result of the measurement is shown in Fig. 14. All three samples have significantly narrower spectrum than previously reported[10] for $In_{0.2}Ga_{0.8}As/Al_{0.38}Ga_{0.62}As$. The difference in spectral width when the well is changed from $L_w = 30$ Å to 40 Å is in excellent agreement with the theoretical calculations. According to the calculations, the first excited state for the 30 Å sample is in the continuum, resulting in a broad absorption spectrum. On the other hand, the excited state in the 35 Å sample is just slightly bound (quasi-bound), and in the 40 Å sample is more strongly bound. In either case, the intersubband absorption for both is narrow and is in excellent agreement with the experimental results. It is known that the spectral width ($\Delta v = 0.13 \mu m$) of the 40 Å well sample is the narrowest reported for a QWIP. Additionally, the detectivity equals
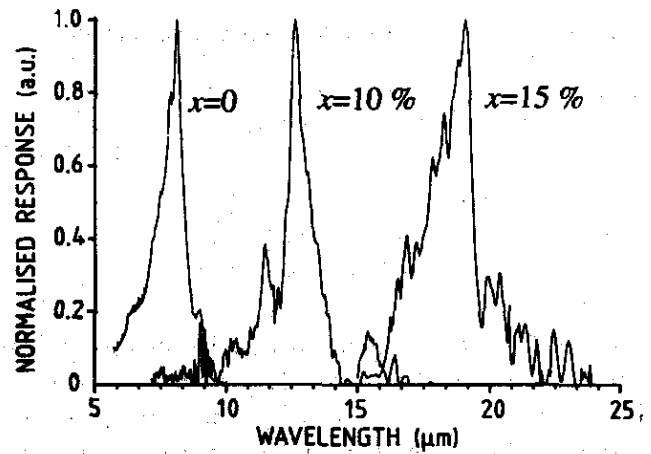
3×10^{10} cmHz$^{1/2}$W^{-1} at 77K and the value of the responsivity is constant up to 200K.

3.3.3 AlGaInAs/InP QWIPs

The band gap of $InGaAlAs$ can be engineered between the two boundary ternary alloys, $In_{0.53}Ga_{0.47}As$ (0.76 eV) and $In_{0.52}Al_{0.48}As$ (1.46 eV). The growth of $InGaAlAs$ alloy is relatively easier[35] than $InGaAsP$ due to: (i)Only one group V element, arsenide, is incorporated, avoiding the problem of As/P ratio control; (ii)composition of the layer is controlled by each constituent element's flux intensity; and (iii)near-unity sticking coefficients of the three group III elements facilitate reproducibility of composition.

For these experiments, three structures were grown by GSMBE with arsine and phosphine as group V sources, elemental gallium and indium as group III sources, and elemental silicon as an n-type dopant source. The $AlAs$ mole fraction in $In_{0.52}(Ga_{1-x}Al_x)_{0.47}As$ and the QW width for the three samples were $(x = 0,56Å)$, $(x = 0.1,60$ Å), and $(x = 0.15, 65$ Å), respectively. Each structure consisted of 20 periods of $InGaAlAs$ QWs separated by 400 Å InP barriers. The QWs were doped $n = 8 \times 10^{17}$ cm^{-3}. Top and bottom 0.6 μm layers of $n = 1 \times 10^{18}$ cm^{-3} $In_{0.53}Ga_{0.47}As$ were grown for ohmic contacts.

The responsivity spectrum of the three samples measured at $T = 10K$ are shown in Fig. 15. For

45

Table 4. Spectral response parameters for the samples A, B and C

Sample	Peak wavelength (μm)	Cut-off wavelength (μm)	FWHM ($\Delta\lambda/\lambda$) (percentage)
A	8.1	8.5	12.5
B	12.7	13.3	8.0
C	19.0	19.5	9.0

a biases of -1V (mesa top negative), the 50 per cent long-wavelength cut-off wavelengths for the three samples were 8.5 μm, 13.3 μm and 19.4 μm, respectively. The peak and cut-off wavelengths, and linewidth $\Delta\lambda/\lambda$ for the three samples are given in Table 4.

The absolute responsivities were measured using a calibrated blackbody source. The detectors were back illuminated through a 45° polished facet. The bias dependence of the responsivity was measured for samples A and B at $T = 77$K and the results are shown in Fig. 16 for both positive and negative biases. The responsivity of sample C was too low to be measured at $T = 77$K. The peak responsivity at -1 V of the $In_{0.52}Ga_{0.38}Al_{0.1}As/InP$ QWIP (sample B) was 0.37 A/W. This is comparable (20 per cent higher) to the $InGaAsP/InP$ QWIP (1.3 μm band gap, $L_w = 63$ Å) reported by Gunapala[36], et al. which had a similar 13.2 μm cut-off wavelength. It is worth noting the responsivity for these samples are approximately five times as large as the best responsivity measured for $GaAs/AlGaAs$ QWIPs.
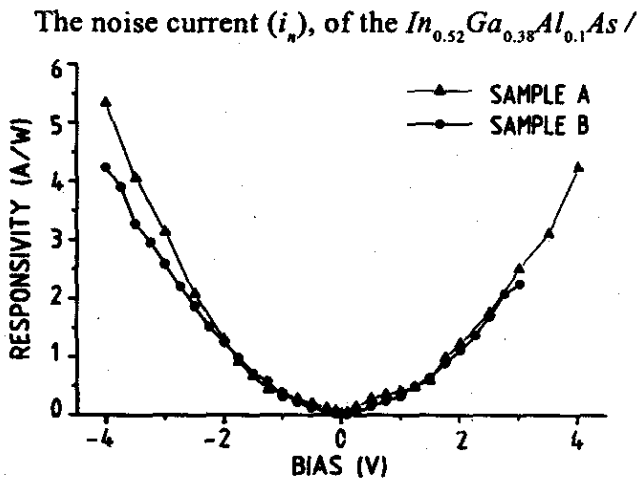
The noise current (i_n), of the $In_{0.52}Ga_{0.38}Al_{0.1}As /$

Figure 16. Bias dependence of peak responsivity measured at T=77K for $InGaAs/InP$ (sample A) and $In_{0.52}Ga_{0.38}Al_{0.1}As/InP$ (sample B) QWIPs.

InP and $In_{0.53}Ga_{0.47}As/InP$ QWIPs were measured at $T = 77$K as a function of bias voltage (V_B) using a spectrum analyser and found to be $i_n = 80$ and 0.4 pA at $V_B = -1$ V. The peak detectivities, D^*_λ can now be calculated from

$$D^*_\lambda = R\sqrt{A\Delta f} / i_n$$

where A=1.6×10^{-4} cm^2 is the device area and Δf=1 Hz is the bandwidth. At an operating $V_B = -1$ V and $T = 77$K, the measured values for the $In_{0.52}Ga_{0.38}Al_{0.1}As/InP$ QWIPs are R_p=0.37 A/W, $i_n = 80$ pA/$\sqrt{\text{Hz}}$ and thus D^*=1x10^9 cm $\sqrt{\text{Hz}}$W^{-1}. The detectivity of the first sample ($GaInAs/InP$ QWIP) at T=77K and $V_B = -1$ V is D^*=4 × 10^{10}cm $\sqrt{\text{Hz}}$W^{-1}.

Using the spectral response data obtained for these samples, it is possible to estimate the conduction band offset for the $In_xGa_{1-x-y}Al_yAs/InP$ heterojunction. The cut-off wavelength for samples A, B and C correspond approximately to the energy separation $\Delta E=E_2-E_1$ for the three aluminium compositions, y = 0 (A), y = 0.1 (B) and y = 0.15 (C). The E_g of $In_{0.52}(Ga_{1-x}Al_x)_{0.48}As$ layers changes linearly from 0.75 eV to 1.47 eV with increasing x as was reported by Fujii,[37] etal. The electron effective mass of $In_{0.52}(Ga_{1-x}Al_x)_{0.48}As$ layers was reported by Olego,[38] et.al. and changes linearly from 0.041m$_0$ to 0.075 m$_0$ with increasing x. In Table 5, the conduction band offset that best fits
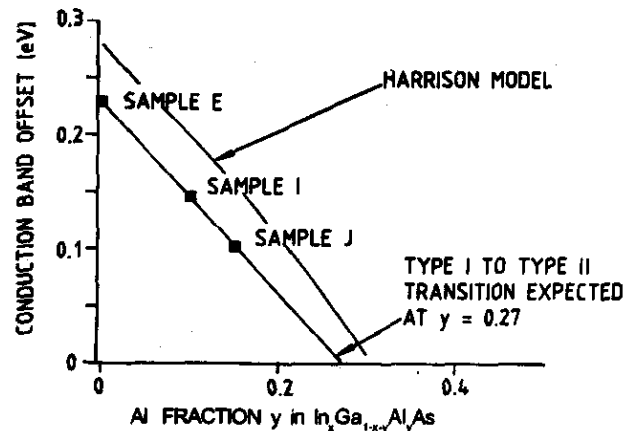

Figure 17. Conduction band offset values calculated from samples A (0 per cent), B (10 per cent), and C (15 per cent) as a function of Al fraction y in $In_xGa_{1-x-y}Al_yAs$. Also shown is a theoretically derived curve[39].

Table 5. Conduction band offset and band offset ratio

Sample	Composition	Well width (Å)	Conduction band offset (ΔE_c) (meV)	Offset ratio $\Delta E_c/E_G$
A	$In_{0.53}Ga_{0.47}As$	56	229	0.370
B	$In_{0.52}Ga_{0.38}Al_{0.1}As$	59	146	0.290
C	$In_{0.52}Ga_{0.36}Al_{0.15}As$	66	103	0.235

the cut-off wavelength observed in Fig. 15 is listed.

A plot of the fit conduction band offset as a function of aluminium fraction is shown in Fig. 17. The data from samples A, B and C are indicated in this figure. The line is the band offset predicted by the Harrison model as applied by Ishikawa[39,40], *et al*.

From the experimental data for these QWIPs, it would be expected that the transition from typeI QW to type II staggered QW for $In_{0.53}(Ga_xAl_{1-x})_{0.47}As/InP$ heterojunctions would occur at $y = 0.27$. This is lower than the value ($y = 0.33$) predicted by the experimental model, which is based on an interpolation from binary data for *InAs*, *GaAs* and *AlAs*, but larger than other recent experimental results for GSMBE-grown material: $y = 0.18$, calculated from interband absorption by Kawamura[41], *et al*., and $y = 0.23$, calculated from Shottky diode dark current by Chua[35], *et al*. Because intersubband absorption is very sensitive to the conduction band offset, the measurements presented here represent an accurate method for determining this typeI QW-to-typeII QW transition composition.

3.4 *GaInAsP/InP* QWIPs

We report the first detailed measurements performed on QWIPs ($\lambda = 8$ μm–20 μm) fabricated from *n*-type *GaInAsP* QWs and *InP* barriers grown by metallo-organic chemical vapour deposition (MOCVD). Three QWIP devices were studied and the device parameters are listed in Table 6, where L_b represents the barrier width, L_w is the well width, and N_d denotes the donor doping concentration of the QWs.

MQW structures were grown in a MOCVD system. The group V source materials were 100 per cent arsenic hydride and phosphine, and the group III source materials were trimethylindium and triethylgallium. All samples were grown on substrate at 480 °C on semi-insulating (100) *InP* wafers. The growth rates of *InP*, *GaInAs*, *GaInAsP* (1.3 μm) and *GaInAsP* (1.5 μm) were 150 Å/min, 300 Å/min, 230 Å/min, and 260 Å/min, respectively. The wells of the MQW structure were silicon doped using silane to a level of 1.7×10^{17} cm^{-3}. Top and bottom contact layers (0.5 μm) of $In_{0.53}Ga_{0.47}As$ doped to $n = 1 \times 10^{18}$ cm^{-3} were grown for ohmic contacts. Arrays of 400 μm × 400 μm mesas were etched through the photosensitive MQW region using a Plasma-Therm 770 ECR/RIE etch system. A mix of $H_2/Ar/Cl_2$ gases was used. Finally, titanium/platinum/gold ohmic contacts were evaporated onto the top and the bottom contact layers.

The relative responsivity spectra for these three samples were collected using a Mattson-Galaxy 3000 FTIR. The responsivity spectrum of the three samples is shown in Fig. 18. For a bias of −1 V (mesa top negative), the 50 per cent cut-off

Table 6. Device parameters for measured QWIPs

QWIP	Sample A	Sample B	Sample C
Barrier material	*InP*	*InP*	*InP*
Barrier width (L_b) (Å)	500	500	500
Well material	$In_{0.625}Ga_{0.375}As_{0.8}P_{0.2}$	$In_{0.73}Ga_{0.27}As_{0.575}P_{0.425}$	$In_{0.53}Ga_{0.47}As$
Well band gap (μm)	1.30	1.55	1.65
Well width (L_w) (Å)	65	65	60
Donor doping density (N_d) (cm^{-3})	1.7×10^{17}	1.7×10^{17}	1.7×10^{17}
Doping concentration (n_s) (cm^{-2})	1.1×10^{11}	1.1×10^{11}	1.0×10^{11}
Periods	20	20	20

Table 7. Spectral response parameters for samples A, B and C

Sample	Peak wavelength (μm)	Cut-off wavelength (μm)	FWHM ($\Delta\lambda/\lambda$) (percentage)
A	12.03	14.24	36.0
B	10.20	10.70	10.0
C	9.00	9.25	5.5

wavelengths for the three samples A, B and C were 9.3 μm, 10.7 μm and 14.2 μm, respectively. The peak and cut-off wavelengths and linewidth $\Delta\lambda/\lambda$ for the three samples are given in Table 7. The switch from a bound-to-bound to a bound-to-continuum transition between samples B and A is evident.

The absolute responsivities were measured using a calibrated blackbody source. The detectors were back illuminated through a 45° polished facet. The bias dependence of the responsivity was measured for three samples. The two samples B and C were measured at T = 80K. Unfortunately, the responsivity of sample A was too low to be measured at T = 80K; instead, the responsivity of this sample was measured at T = 30K. The peak responsivity for the three samples is shown in Fig. 19.

The peak responsivity at –1 V of the samples A, B and C were 28.1 mA/W, 71.8 mA/W and 11.8 mA/W, respectively. The i_n of samples B and C were measured at T = 80K and sample A was measured at T = 30K. The i_n was measured using a spectrum analyser and found to be 10 pA,
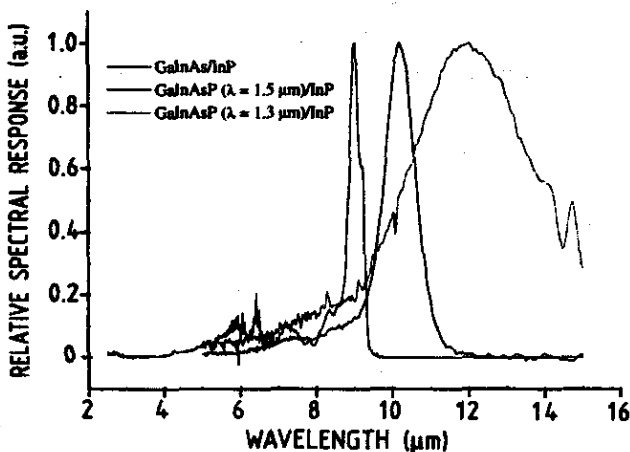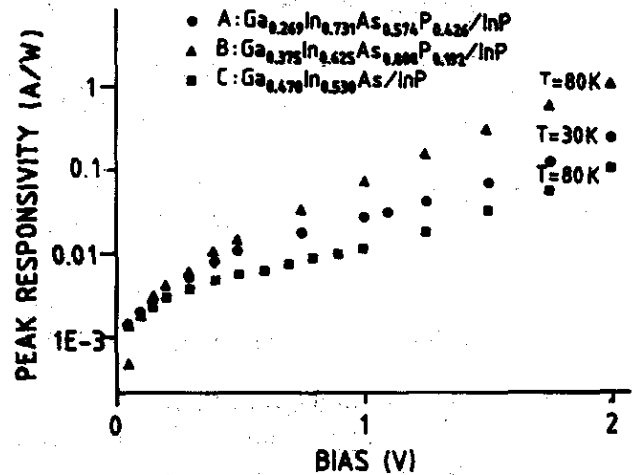

Figure 19. Peak responsivity measured as a function of bias for samples A, B and C.

4.4 pA, and 62 fA, respectively for samples A, B and C. The peak detectivities, D^*_λ can now be calculated from the following expression

$$D^*_\lambda = R\sqrt{A\Delta f} / i_n$$

where A = 1.6 × 10⁻³ cm² is the device area and Δf = 1 Hz is the bandwidth.

At an operating bias V_B = –1 V and T = 80K, the detectivity for samples B and C are D^* = 2 × 10⁸ cm √HzW⁻¹ and 8 × 10⁹ cm √HzW⁻¹, respectively. The detectivity of the sample A at T = 30K is D^* = 1.1 × 10⁸ cm √HzW⁻¹ The detectivity of the three samples as a function of

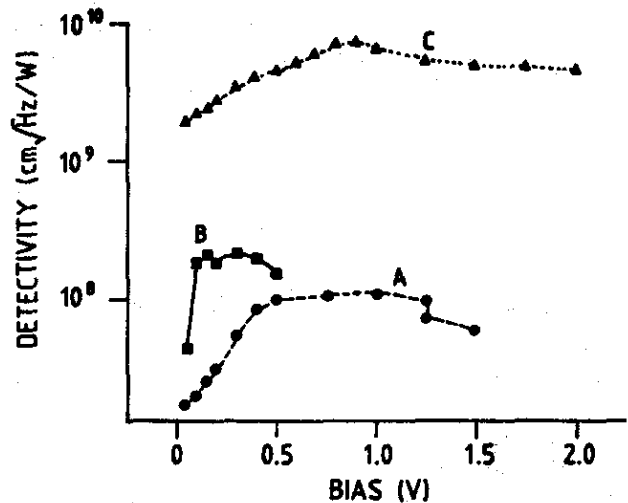Figure 18. Relative spectral responses for samples A, B and C.

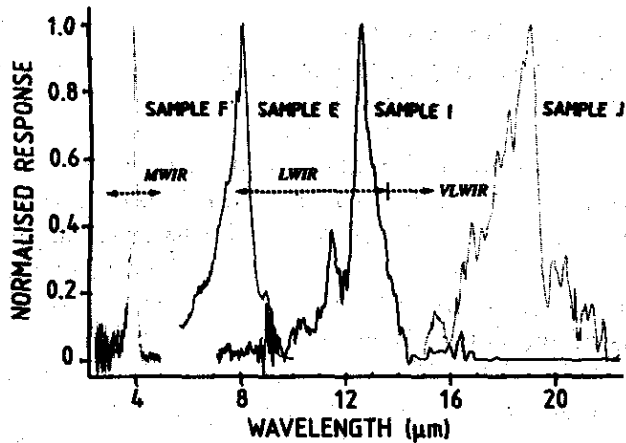Figure 20. Specific detectivity as a function of bias for samples A (O) , B (□), and C (△).

Figure 21. QWIP detectors lattice- matched to *InP* can cover the entire range from 3 μm-20 μm, using the spectral response for samples A, B, C and D.

bias is shown in Fig. 20.

Using the spectral response data obtained for these samples, it is possible to estimate the conduction band offset for the $Ga_xIn_{1-x}As_yP_{1-y}/InP$ heterojunction. The cut-off wavelength for samples A, B and C correspond approximately to the energy separation $\Delta E = E_2 - E_1$ for the three quaternary compositions: Sample A $(x, y) = (0.270, 0.575)$, sample B $(x, y) = (0.375, 0.800)$ and sample C $(x, y) = (0.470, 0)$. The energies of the first and second allowed states for these *GaInAsP/InP* samples can be calculated for several possible conduction band offsets using the

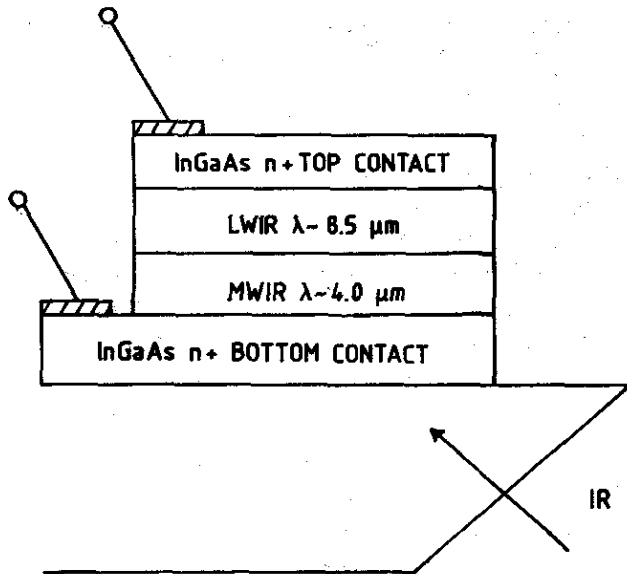

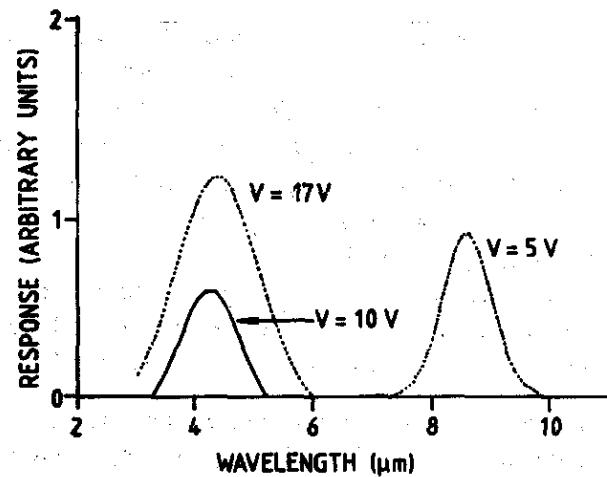Figure 22. Multispectral QWIP design used for measuring sample K.

Figure 23. Response for wafer K at *T*=77K for several biases. (For V < 7 volts, only one peak at ~ 8.5 μm is observed. For higher biases, a peak at ~ 4 μm is measured).

well widths given in Table 6. The conduction band offset ratios $(\Delta E_c/\Delta E_g)$ that best fit the cut-off wavelengths observed in Fig. 18 for samples A, B, and C are 0.32, 0.30 and 0.33, respectively. It is nearly constant for all three samples, with an average value of ~ 0.32. This value for the *GaInAsP/InP* conduction band offset is smaller than the previously reported value[42,43] of 0.40.

3.5 Multispectral QWIPs

As we have shown earlier, QWIP lattice-matched to *InP* substrate can be used for detection in the MWIR, LWIR, and very long-wavelength infrared (VLWIR) spectral regions. Figure 21 shows the combined relative spectral responses for samples A, B, C and D as a function of wavelength. The MWIR and LWIR regions of high atmospheric transmission are indicated by arrows. Multispectral detectors lattice-matched to *GaAs* substrate, using the *GaAs/AlGaAs* and *InGaAs/AlGaAs* systems have been previously reported. In this section, we report the first multispectral detectors on *InP* substrate.

A sample (wafer K) was grown for multispectral absorption in both MWIR and LWIR regions by including multiple QWs of both *InGaAs/InAlAs* and *InGaAs/InP*. The QWIP structure was grown on (100) oriented semi-insulating (iron-doped) *InP* substrates. The first layer is an 1 μm buffer layer of n^+ *InGaAs* doped with silicon to $n = 1 \times 10^{18}$ cm^{-3}. This served a bottom contact.

49

Next grown was two series of MQWs. The first consisted of 21 barrier layers of *InP* (500 Å) confining 20 wells of $In_{0.53}Ga_{0.47}As$ (55 Å). The second consisted of 21 barrier layers of $In_{0.52}Al_{0.48}As$ (350 Å) confining 20 wells of $In_{0.53}Ga_{0.47}As$ (35 Å). Last grown was a 0.5 μm top contact layer of n^+ $In_{0.53}Ga_{0.47}As$ (silicon doped to $n = 1 \times 10^{18}$ cm^{-3}). For this sample, the 2 Å nearest each barrier remained undoped. The remainder of the well was doped to a concentration, $n = 5 \times 10^{17}$cm^{-3}.

Detectors from wafers K were fabricated using the Plasma-Therm ECR/RIE dry etching system. Because the mask utilised in this study allows only one contact to be made to the mesa, the two MQW detectors were placed in series. At low biases, the electric field was applied mostly across the lower-resistance *InGaAs/InP* MQW. At higher biases, the electric field was applied across both the MQWs, but the *InGaAs/InP* MQW is under such high electric field that no response was observed. This is because most carriers in the ground states of the *InGaAs/InP* QWs tunnel out before absorption occurs. A schematic of the device is shown in Fig. 22.

The spectral response of detectors from wafer K are shown in Fig. 23 for several biases. For biases < 10 V, the photoresponse in the 3 μm-5 μm region is too noisy to resolve. For biases > 7 V, the photoresponse in the 8 μm-9 μm region is no longer observed.

Because only one mask set was available for this study, the multispectral QWIPs presented in this section operate as a voltage-tunable detector, rather than as a true simultaneous multispectral detector. Nonetheless, the feasibility of integrating MW, LW and/or VLW QWIPs based on *InP* into a multispectral imaging array has been demonstrated.

4. CONCLUSIONS

We have characterised and optimised the performance of QWIP fabricated from QWs or barriers of *GaInAlAs* or *GaInAsP* material and made a comparison with that achieved with the more mature *GaAs/AlGaAs* device design. To demonstrate new functionality, such as the possibility of multispectral detection, we have investigated several designs based on heterostructures of *GaAs/GaInP*, *InGaAs/InP*, *InGaAs/InAlAs* and *AlGaInAs/InP*.

This study has enabled us to deduce from the QWIP devices fabricated from *GaAs/GaInP*, several important parameters describing this heterostructure system. A precise value for the conduction band discontinuity of 122 meV ±2 meV was calculated. A drift mobility of 1000 cm^{2}V^{-1}s^{-1}, saturation velocity of 1.5×10^5 cm^{-1}, and carrier lifetime of ~ 5 ps have also been extracted from the current-voltage curves. Although it is clear that the conduction band offset in this system is too small for 8 μm-12 μm devices, excellent VLWIR detectors were produced with performance equivalent to *GaAs/AlGaAs* detectors at the same wavelength.

Three identical *GaInAs/InP* QWIP series ($\lambda = 9$ μm) were grown by LP-MOCVD with three different QW doping densities. The optimal detectivity came from the series with $N_d = 5 \times 10^{17}$ cm^{-3}. This series had a responsivity of 33.2 AW^{-1} and operated with a detectivity of 3.5×10^{10} cmHz$^{1/2}$W^{-1} at a bias of 0.75 V. This responsivity is the highest known value reported for any QWIP in the $\lambda = 8$ μm–9 μm range.

We presented optimisation of the device design for *InGaAs/InAlAs* QWIP for MWIR detection. These MWIR detectors demonstrate high detectivity, and have a constant responsivity up to $T = 200$K. The fact that they are lattice-matched to *InP* has allowed to demonstrate the first *InP*-based multispectral detector for 3 μm-5 μm and 8 μm-9 μm detection. In addition, QWIP fabricated from the *AlGaInAs/InP* material system have been presented that are sensitive to the spectral region between $\lambda = 8$ μm–20 μm when the aluminium mole fraction is varied from 0 per cent–15 per cent.

Lastly, we have demonstrated the first preliminary QWIP detectors using the quaternary *InGaAsP/InP* materials system growth by MOCVD. By increasing the band gap from ternary *InGaAs* to quaternary *InGaAsP*, we have shifted the responsivity out to longer wavelengths resulting in cut-off wavelengths

of 10.7 μm and 14.2 μm for arsenic mole fractions of 0.80 and 0.57, respectively. For the device with a 10.7 μm cut-off wavelength, we observed responsivity as large as 1.09 A/W at a bias of 2V. The conduction band offset for these samples is ~ 0.32, lesser than the typically reported value of 0.40.

ACKNOWLEDGEMENTS

REFERENCES

1. Esaki, L. & Sakaki, H. *IBM Tech. Disc. Bull.*, 1977, **20**, 2456.

2. West, L. & Eglash, S. *Appl. Phys. Lett.*, 1985, **46**, 1156.

3. Levine, B.F.; Choi, K.K.; Bethea, C.G.; Walker, J. & Malik, R.J. *Appl. Phys. Lett.*, 1987, **50**, 1092.

4. Kukkonen, C.A.; Gunapala, S.D.; Bandara, S.V.; Liu, J.K. & Llorens, J. *Proceedings SPIE*, 1999, **3698**, 706.

5. Jelen, C.; Slivken, S.; Guzman, V.; Razeghi, M. & Brown, G.J. *IEEE J. Quant. Electron.*, 1998, **34**, 1873.

6. Jelen, C.; Slivken, S.; David, T.; Brown, G. & Razeghi, M. *Proceedings SPIE*, 1998, **3287**, 96.

7. Gunapala, S.D.; Levine, B.F.; Ritter, D.; Hamm, R. & Panish, M.B. *Appl. Phys. Lett.*, 1991, **58**, 2024.

8. Andersson, J.Y.; Lundqvist, L.; Paska, Z.F.; Streubel, K. & Wallin, J. *Proceedings SPIE*, 1992, **1762**, 216.

9. Levine, B. *J. Appl. Phys.*, 1994, **74**, R1.

10. Chen, C.; Choi, K.; Tidrow, M. & Tsui, D. *Appl. Phys. Lett.*, 1996, **68**, 1446.

11. Hasnain, G.; Levine, B.; Sivco, D. & Cho, A. *Appl. Phys. Lett.*, 1990, **56**, 770.

12. Rogalski, A. *Infrared Phys. Technol.*, 1999, **40**, 279.

13. Tung, T.; DeArmond, L. V.; Herald, R. F.; Herning, P. E.; Kalisher, M. H.; Olson, D. A.; Risser, R. F.; Stevens, A. P. & Tighe, S.J. *Proceedings SPIE*, 1992, **1735**, 109.

14. Arias, J. M.; Zandian, M.; Pasko, J. G.; Bajaj, J.; Kozlowski, L. J.; Tennant, W. E. & de Wames, R. E. *Proceedings SPIE*, 1994, **2274**, 2.

15. Chang, Y. C. & James, R. B. *Physical Review B: Solid State*, 1989, **39**, 12672.

16. Levine, B. F.; Hasnain, G.; Bethea, C. G. & Chand, N. *Appl. Phys. Lett.*, 1989, **54**, 2704.

17. Razeghi, M. MOCVD challenge, Vol. 2. Institute of Physics Publishing, Bristol, 1995. pp.22-49.

18. Hasse, M.; Hafich, M. & Robinson, G. *Appl. Phys. Lett.*, 1991, **58**, 616.

19. Razeghi, M.; Defour, M.; Ohmnes, F.; Dobers, M.; Vieren, J. & Guldner, Y. *Appl. Phys. Lett.*, 1989, **55**, 457.

20. Olson, J.M.; Ahrenkiel, R.K.; Dunlavy, D.J.; Keyes, B. & Kibbler, A.E. *Appl. Phys. Lett.*, 1989, **55**, 1208.

21. Mitchel, W.C.; Brown, G.J.; Lo, K.; Elhamri, S.; Ahoujja, M.; Ravindran, K.; Newrock, R.; He, X. & Razeghi, M. *Appl. Phys. Lett.*, 1994, **65**, 1578.

22. Andrews S. & Miller, B. *J. Appl. Phys.*, 1991, **70**, 993.

23. Dicke, R.H. & Wittke, J.P. Introduction to quantum mechanics. London, UK: Addison-Wiley, 1960.

24. Wolfe, W. L. & Zeiss, G. J. The Infrared handbook. Environmental Research Institute of Michigan, Ann Arbor, MI, 1985.

25. Brennan, K.F. & Chiang, P. *J. Appl. Phys.*, 1992, **71**, 1055.

26. Masselink, W.; Braslau, N.; Tulipe, D. La; Wang, W. & Wright, S. *Solid-State Electron.*, 1988, **31**, 337.

27. Kane, M. J.; Millidge, S.; Emeny, M.T.; Lee, D.; Guy, D.R.P. & Whitehouse, C.R. *In* Intersubband transitions in quantum wells, edited by E. Rosencher; B. Vinter and B. Levine. Plenum, New York, 1992. pp.31–42.

28. Jelen, C.; Slivken, S.; David, T.; Razeghi, M. & Brown, G. J. *IEEE J. Quant. Electron.*, 1998, **34**, 1124.

29. Razeghi, M. MOCVD challenge, Vol. 1. Adam Hilger, Bristol, 1989. pp. 8–24.

30. Chuang, S. L. Physics of optoelectronic devices. John Wiley & Sons, New York, 1995. pp. 31–35.

31. Kinch, M. A. & Yariv, A. *Appl. Phys. Lett.*, 1989, **55**, 2093.

32. Gunapala, S. D.; Levine, B. F.; Pfeiffer, L. & West, K. *J. Appl. Phys.* 1991, **69**, 6517.

33. Hasnain, G.; Levine, B. F.; Gunapala, S. & Chand, N. *Appl. Phys. Lett.*, 1990, **57**, 608.

34. Gunapala, S.D.; Liu, J.K.; Park, J.S.; Sundaram, M.; Shott, C.A.; Hoelter, T.; Lin, T.; Massie, S.T.; Maker, P.D.; Muller, R.E. & Sarusi, G. *IEEE Trans. Electron. Devices*, 1997, **44**, 51-57.

35. Chua, S.J. & Ramam, A. Proceedings of the 1996 IEEE International Conference on Semiconductor Electronics, ISDE. Piscataway, NJ, SPIE Press, 1994. pp.469-71.

36. Gunapala, S. D.; Levine, B. F.; Ritter, D.; Hamm, R. A. & Panish, M. B. *Appl. Phys. Lett.*, 1992, **60**, 636.

37. Fujii, T.; Nakata, Y.; Sugiyama, Y. & Hiyamizu, S. *Jpn. J. Appl. Phys.*, Part II, 1986, **25**(3), L254-L256.

38. Olego, D.; Chang, T.Y.; Silberg, E.; Caridi, E.A. & Pinkzuk, A. *Appl. Phys. Lett.*, 1982, **41** (5), 476-78.

39. Ishikawa, T. & Bowers, J.E. *IEEE J. Quant. Electron.*, 1994, **30**(2), 562-70.

40. Harrison, W.A. *J. Vac. Sci. Technol.* 1977, **14**(4), 1016-21.

41. Kawamura, Y.; Kobayahsi, H. & Iwamura, H. *Jpn. J. Appl. Phys.*, (Part II), *Lett.* 1994, **33**(1B), L79-L82.

42. Soucail, B.; Voisin, P.; Voos, M.; Rondi, D.; Nagle, J. & Crémoux, B.de *Semicond. Sci. Technol.*, 1990, **5**, 918.

43. Cavicchi, R. E.; Lang, D. V.; Gershoni, D.; Sargent, A. M.; Vandenberg, J. M.; Chu, S. N. G. & Panish, M. B. *Appl. Phys. Lett.*, 1989, **54**, 739.